Materials Science-Poland, Vol. 22, No. 2, 2004

Synthesis and characterization of metastable CeO_2–ZrO_2 solid solution obtained by polymerized complex method

WŁODZIMIERZ MIŚTA[1,*], TREVOR RAYMENT[2], JERZY HANUZA[1], LUCYNA MACALIK[1]

[1]Institute of Low Temperature and Structure Research,
Polish Academy of Sciences, P.O. Box 1410, 50-950 Wrocław 2, Poland

[2]Chemistry Department, Cambridge University, Cambridge CB2 1EW, UK

The paper describes the preparation and characterization of nano-size metastable tetragonal CeO_2 –ZrO_2 mixed oxides prepared by a polymerized complex method. A glycine–ethylene glycol solution containing Ce^{3+} and Zr^{4+} ions was polymerized at 80–110 °C to form a viscous transparent resin without any visible precipitation. After heat-treatment at relatively low temperature (ca 250 °C) on a hot plate in static air, the solid precursor ignited in part due to self-combustion, resulting in the formation of a nanocrystalline, compositionally-homogeneous solid solution. Its structure was confirmed using X-ray diffraction, HRTEM and Raman spectroscopy. The phase separation in CeO_2–ZrO_2 system on a subsequent heat-treatment in air and in a mixture of H_2 and He was also investigated up to 1100 °C.

Key words: *ceria–zirconia; polymerized complex method; Raman spectroscopy; X-ray diffraction*

1. Introduction

Cerium oxide, as a non-stoichiometric rare-earth oxide, has been extensively used in heterogeneous catalysis [1]. Ceria-based mixed oxides are active components of three-way automotive catalysts (TWC) [2–7]. One of the most important roles of CeO_2 in these systems is their ability to store and release oxygen which is related to their redox properties and thermal stability; oxygen storage capacity (OSC) of these materials increases significantly when Zr^{4+} is doped into CeO_2 lattice. A considerable decrease of bulk reduction temperature of mixed CeO_2–ZrO_2 solid solutions is caused by a strong modification of the oxygen sublattice which generates mobile oxygen atoms [8–10].

* Corresponing author, e-mail: mista@int.pan.wroc.pl.

The traditional method for the preparation of multicomponent materials involves preparation of mechanically mixed oxides powders which are subjected to high -temperature calcination for several hours to homogenize the ceria–zirconia composition via solid state reactions. However, this method gives materials with very low surface area and often yields compositional inhomogeneities. To overcome the need for high temperature homogenization in the preparation of $Ce_xZr_{1-x}O_2$ solid solutions, a novel method utilizing room-temperature high-energy mechanical alloying of pure CeO_2 and ZrO_2 has been developed [11, 12]. However, more homogenous compounds are generally prepared via co-precipitation techniques [13–17], hydrothermal synthesis [18–21], spray pyrolysis [22], physical gelation [23, 24], solution combustion [25, 26], sol-gel [27] and the microemulsion methods [28, 29].

The purpose of this study is to apply the polymerized complex method to the synthesis of nanocrystalline ceria–zirconia solid solutions. This technique is a modified version of the Pechini polymeric precursor method [30–33] and is based on the "in situ" polymerization of ethylene glycol in the presence of simple metal salts complexed by glycine. Such a preparation procedure enabled us to obtain homogenous transparent and very stable polymeric sols. It is very cheap and holds a number of advantages over the popular but rather expensive sol-gel synthesis via alkoxide route in which a dry nitrogen atmosphere must be used and the sols have a limited shelf-life. The sols produced via the polymer route may also be good candidates for the preparation of thin, dense ceria–zirconia films for thermal barrier coatings and in intermediate temperature solid oxide fuel cells (SOFC) [34, 35]. In the present study, we tried to check the homogeneity of the prepared solid solutions and to characterize the phase separation during heat treatment in air and in reducing environment by means of powder X-ray diffraction (XRD), HRTEM and Raman spectroscopy.

2. Experimental

Cerium nitrate hexahydrate $Ce(NO_3)_3 \cdot 6H_2O$ (99.99%, Aldrich) and zirconium oxychloride octahydrate $ZrOCl_2 \cdot 8H_2O$ (99.99%, Aldrich) were weighed to give 0.02 mole final oxide in the defined molar ratio, and mixed with 10 ml distilled water, 10 ml of concentrated nitric acid, 0.02 mole of glycine and 40 ml of ethylene glycol. The colourless clear solution thus obtained was heated on a hot plate at about 80–110 °C in order to expel water and other volatile compounds. As the solution became concentrated, it became viscous and changed colour from colourless to yellow or brown, indicating formation of a polymeric gel. The viscous polymeric product thus obtained was first carefully dried at 140 °C on a hot plate under infrared lamp giving an organic-inorganic solid precursor. After prolonged drying at higher temperatures, the dark brown solid ignited in part due to self-combustion during this process, resulting in formation of yellow powder. The samples were then heated in air in an electric furnace up to 1100 °C for 16 h.

Reduction treatments were performed at 1100 °C in 5% H_2/He flowing at 50 $cm^3 \cdot min^{-1}$ for 5 h in a ceramic tubular furnace. The heating rate was 10 deg/min. Research-grade purity gas mixtures (>99.996%) were employed without further purification. After reduction, partly dark blue samples were cooled down to the room temperature under hydrogen.

XRD patterns were obtained with a Philips PW1830 diffractometer ($Cu_{K\alpha}$ with a graphite monochromator situated behind the sample). X-ray powder diffraction patterns were refined and analyzed by the Rietveld method (DBWS 9807 [36] and PowderCell ver.2.3 [37] software) to determine the amount of different phases as well as their lattice parameters and crystallite size. *In-situ* high-temperature X-ray diffraction (HTXRD) work was carried out using an Anton Paar furnace with Pt/Rh heating strip.

Thermal decomposition of the precursors was studied by thermogravimetry (TG/DTA) using MOM-Budapest equipment. During the TG-DTA measurement, the samples were heated in air up to 1000 °C with heating rate of 10 °C/min.

The room temperature Raman spectra were measured with the Bruker RFS 100 FT-Raman Spectrometer using the back scattering arrangement. The resolution was 2 cm^{-1}. Excitation was performed by 1064 nm line of Nd:YAG laser.

HRTEM image was obtained with a Philips CM 20 microscope equipped with the SuperTwin objective lens and operated at 200 kV.

3. Results and discussion

3.1. Synthesis of CeO_2–ZrO_2 organic-inorganic precursor

The inorganic-organic sols obtained with the polymerized complex method give very stable, transparent, viscous solutions without any evidence of the precipitation. In an ethylene glycol medium, formation of ester bonds between carboxylate groups of glycinato-metal complexes and alcohol groups of ethylene glycol could be possible. Ester bonds would cross-link glycinato-metal complexes into low molecular weight oligomers and thereby prevent precipitation. Inorganic-organic hybrid polymers obtained in such a way consist of a dual polymer network, in which cluster or oligomer-type inorganic structures are linked by organic groups or polymer fragments of polyethylene glycol (PEG). This kind of immobilization of a metal complex into a macrofunctionalized organic ligand (PEG) is responsible for high stability of such systems.

3.2. Crystallization behaviour and thermal analysis

After drying on a hot plate at 140 °C the dark-brown solid inorganic-organic precursors were amorphous as could be seen in Fig. 1 where *in-situ* XRD patterns of the $Ce_{0.5}Zr_{0.5}O_2$ precursor during heat-treatment up to 500 °C with a heating rate of 10 °C/min are presented. Crystallization of the amorphous matrix starts at about 250 °C.

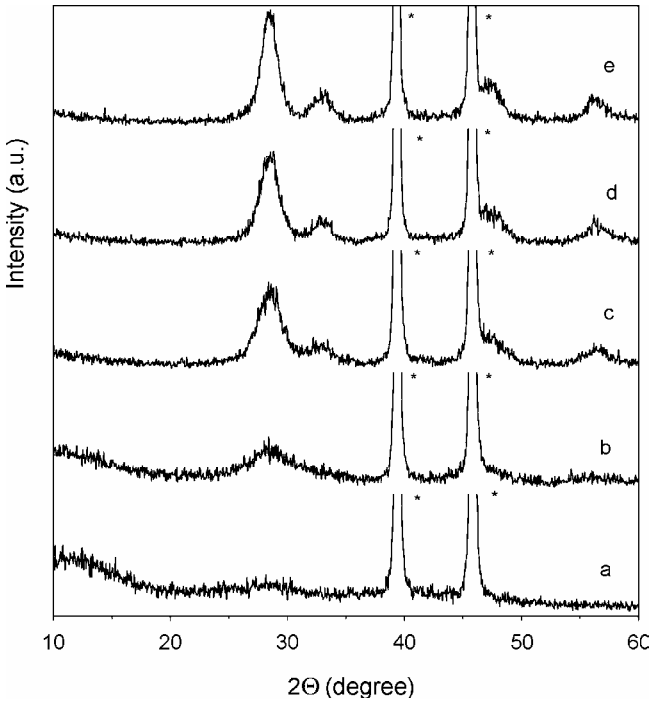

Fig. 1. *In-situ* X-ray diffraction patterns of $Ce_{0.5}Zr_{0.5}O_2$ precursor sample heated at: a) 200 °C, b) 250 °C, c) 300 °C, d) 400 °C, e) 500 °C. Asterisks indicate the Pt/Rh heating strip

Typically, we focused our attention on samples $Ce_{0.3}Zr_{0.7}O_2$ and $Ce_{0.5}Zr_{0.5}O_2$ in order to evaluate thermal evolution of the precursor samples. The differential thermal analyses (DTA) and thermal gravimetric analyses (TG) of gently dried $Ce_{0.3}Zr_{0.7}O_2$ and $Ce_{0.5}Zr_{0.5}O_2$ gels are shown in Figs. 2a, b, respectively. It has been observed that there are three major weight losses of 12.3, 24.7 and 26.0% for $Ce_{0.3}Zr_{0.7}O_2$ and 52.0, 27.0 and 6.0% for $Ce_{0.5}Zr_{0.5}O_2$ precursors. The first weight loss is probably mostly due to dehydration and evaporation of volatile organic components up to 220 °C. The second very rapid weight loss between 220 and 235 °C can be mainly ascribed to exothermic self-combustion reaction of suitable oxidizers (such as metal nitrates) and an organic fuel (such as glycine). The decomposition of glycine–metal nitrate complexes is highly exothermic [38] and the *in-situ* heat generated is utilized for the formation of complex oxides. Similar TG-DTA results were found by Patil et al. [26] during solution combustion (SC) synthesis of complex metal oxides using urea, glycine or hexamethylenetetramine as organic fuels and metal nitrates as oxidizers. The crystallization of amorphous CeO_2–ZrO_2 mixed solid solution starts at about 250 °C (Fig. 1b) which corresponds also to weak exothermic peak which is not well-defined on DTA curve (Fig. 2). The third weight loss extending up to ~500 °C may be due to burnout of most isolated carbon residue and after that there is no further weight loss above 500 °C up to 1000 °C. Products after calcining the gel at 600 °C were crystalline and

resulted in a pale yellow powder. The total weight losses of the polymeric precursors during heating up to 1000 °C were ca. 63% (Fig. 2a) and ca. 85% (Fig. 2b).

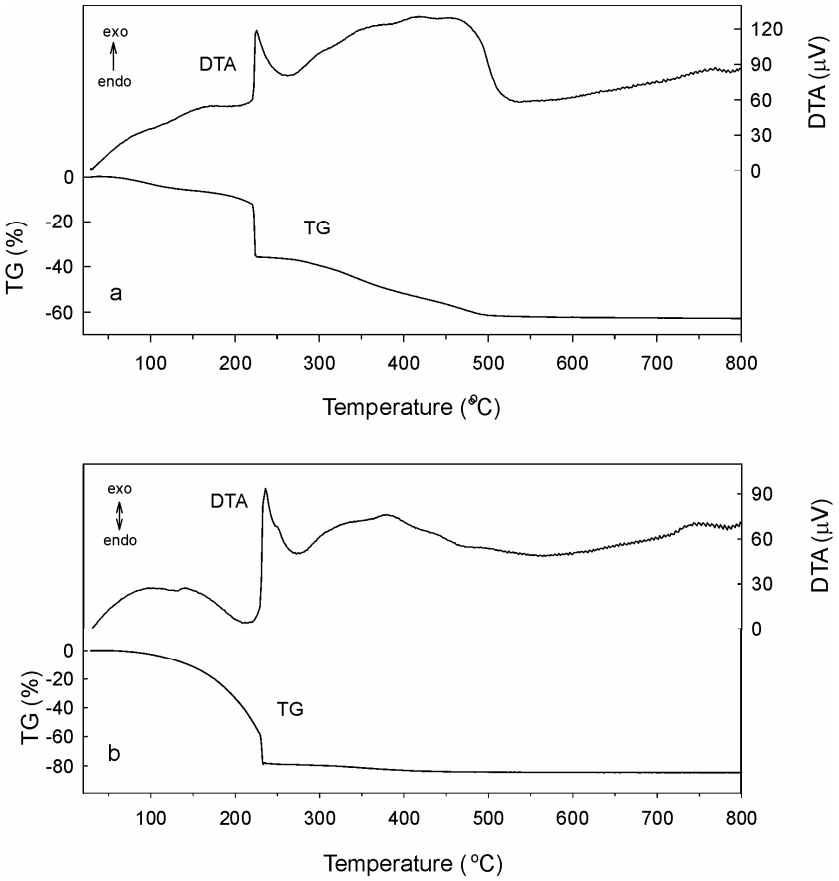

Fig. 2. Differential thermal analysis and thermogravimetric curve of polymeric precursors for samples of: a) $Ce_{0.3}Zr_{0.7}O_2$, b) $Ce_{0.5}Zr_{0.5}O_2$

The DTA curves for the same samples show broad endothermic peak at about 100–220 °C related probably to the dehydration and evaporation of high-melting polymeric compounds like poly(ethylene glycol) (PEG) and subsequently a narrow exothermic peak at 227 °C for $Ce_{0.3}Zr_{0.7}O_2$ or 232 °C for $Ce_{0.5}Zr_{0.5}O_2$ corresponding to the sudden weight loss observed on TG curve which can be attributed to the self-combustion process connected with exothermic redox reaction of suitable oxidizer (metal nitrate) and an organic fuel [26]. The other very broad exotherm at about 270–530 °C could be ascribed to the complete burnout of the residual organic char.

Thermolysis of organic-inorganic gel precursors is a very complex process resulting in complete breakdown of the gel structure before oxide formation. The cation homogeneity is controlled mainly by the thermal stabilities of the metal–glycinate

bridges in different glycinato-metal complexes which could decompose at different temperatures, resulting in phase separation during gel thermolysis [39]. In our case, the organic decomposition takes place simultaneously at a narrow temperature range during self-combustion process. During this process, a large amount of energy has been released resulting in an increase of local temperature. Therefore the Ce- and Zr-glycinate complexes crosslinked to the PEG oligomers undergo a rapid decomposition in the same temperature range. This highly exothermic process enables simultaneous nucleation and crystallization of a highly compositional homogeneous nanocrystalline mixed oxides as observed during the *in-situ* XRD experiment.

3.3. XRD, HRTEM and Raman characterization of the CeO_2–ZrO_2 solid solution

Figure 3 shows XRD patterns of the as-received nanocrystalline $Ce_xZr_{(1-x)}O_2$ samples heat-treated in air at 600 °C for 16 h. The lattice constants and crystallite sizes of each phase are presented in Table 1. The data were analysed using full pattern profile refinement.

For undoped nanocrystalline ZrO_2 sample (Fig. 3) there are two phases, monoclinic and small amount (~8 wt. %) of tetragonal phase. It is well known that undoped t-ZrO_2 could be stabilized by fine crystallites; the increase of their sizes with annealing treatment above 400 °C induces a martensitic t → m phase transition. A simultaneous presence of the tetragonal and monoclinic ZrO_2 was clearly detected with increasing crystallite sizes. Our results are in good agreement with those reported by Djurado et al. [40] who estimated the critical size to be around 23 nm. In our situation after heat-treatment at 600 °C for 16 h, the transformation is almost complete, the content of m-ZrO_2 phase being about 92 wt. % and crystallite size amounting to 27 nm.

Slightly asymmetric XRD profiles for nanocrystalline $Ce_xZr_{(1-x)}O_2$ (x = 0.1–0.2) samples suggest the formation of t-phase (Fig. 3). At 30–40 mol % of CeO_2 the samples mainly consist of t′-phase. The axial ratio c/a decreases with an increase of the content of CeO_2 and became unity at about 50 mol % of CeO_2. The composition $Ce_{0.5}Zr_{0.5}O_2$ represents a further point of interest since it is located at the limit of the t″ → t′ transition which allows one to prepare either tetragonal or cubic form by simply changing the preparation conditions [29, 41, 42]. A pseudocubic t″ phase mainly exists in the range of 50–80 mol % of CeO_2 content (Fig. 3, Table 1). The lattice parameters for cubic (t″, c) nanocrystalline $Ce_xZr_{(1-x)}O_2$ (x = 0.5–1.0) samples demonstrate rather good linear relationship between the cell parameters and the ZrO_2 content. However, the comparison between various literature data, in particular when different synthesis methods are employed, leads to a significant disagreement between the data [11, 41]. Since XRD patterns of nanocrystalline $Ce_xZr_{(1-x)}O_2$ solid solution are remarkably broad and sensitive mainly to the cation sublattice, it is very difficult to find the accurate phase composition.

The crystal structures and phase transformations in the CeO_2–ZrO_2 binary system have been investigated by many researchers [9, 43–48]. However, we are not aware of

any detailed and systematic study of the of nanostructured $Ce_xZr_{(1-x)}O_2$ materials prepared by the low-temperature method over the entire composition range. In the intermediate region, the exact nature of the phases is still unclear, because of stable and metastable phases of tetragonal symmetry present [41, 49]. Only arc-melted CeO_2 –ZrO_2 powders have been carefully studied by Yashima et al. [43–45, 50].

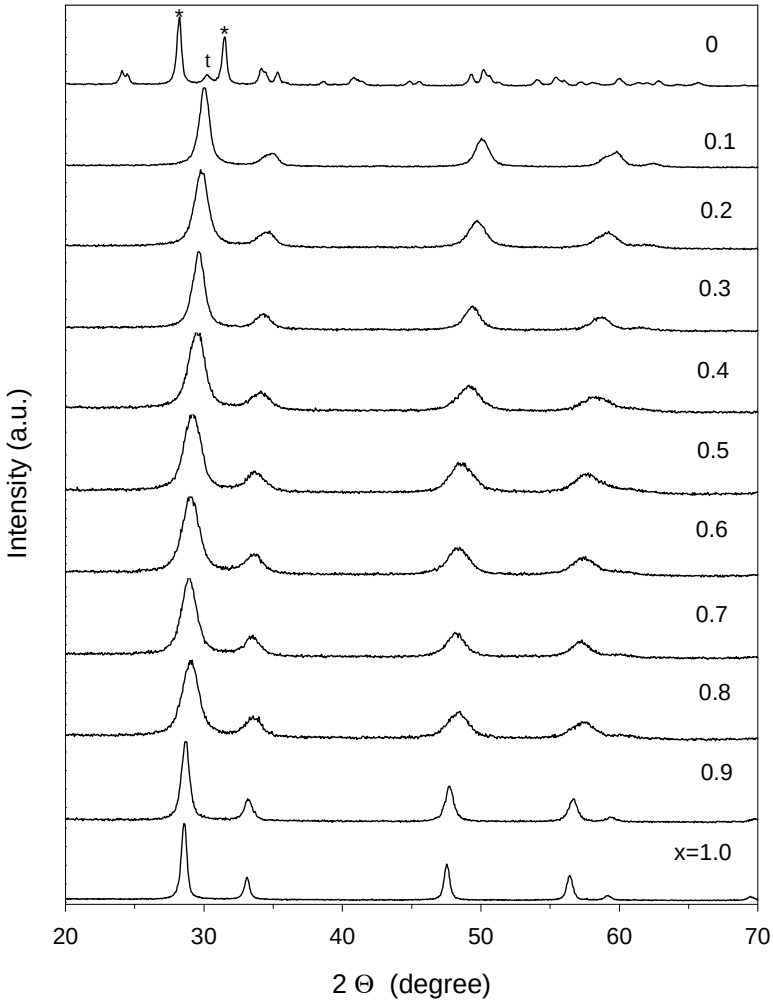

Fig. 3. X-ray diffraction patterns of $Ce_xZr_{(1-x)}O_2$ samples heated in air at 600 °C for 16 h. The symbols * and t indicate most intense lines of the monoclinic and tetragonal phases, respectively

One of the characteristic features of the zirconia–ceria solid solutions prepared by solid state reaction at high temperatures is the existence of monoclinic, cubic (fluorite type) and three tetragonal forms (t, t′, t″), all belonging to the $P4_2/nmc$ space group. At high cerium oxide concentrations, the cubic phase is formed, whereas for the zirconia-rich solid solution the monoclinic phase appears. A stable tetragonal form is

called the t-form, which is restricted to the solubility limit predicted by the equilibrium phase diagram. There is also a metastable t′-form with a wider solubility, but unstable with respect to the mixture of the t-form and the cubic phase. Finally, another metastable t″-form has an axial ratio *c*/*a* of unity, but with the oxygen atoms displaced along the c-axis from their ideal sites of the cubic phase (8*c* sites of the *Fm*3*m* space group). The t′/t″ and t″/c boundaries have been investigated by many authors [9, 10, 41, 43, 51] but the exact positions of metastable tetragonal regions strongly depend on the crystallite size and the synthetic method employed in preparation.

XRD patterns of the nanocrystalline $Ce_xZr_{(1-x)}O_2$ (x = 0.2–0.8) solid solutions calcined at 600 °C (Fig. 3) present very broad reflections. The average crystallite sizes of $Ce_xZr_{(1-x)}O_2$ (x = 0.2–0.8) samples give values of approx. 8–10 nm (Table 1). The addition of ZrO_2 in the form of solid solution resulted in effective improving the thermal stability of CeO_2 [41, 47, 48]. A pure ceria tends to sinter rapidly during heat-treatment at 600 °C yielding crystallite size about 23 nm (Table 1).

Table 1. XRD Characterization of $Ce_xZr_{1-x}O_2$ samples calcined at 600 °C for 16 h

CeO_2 [mol %]	Lattice type	Lattice parameters [Å]	D^c [nm]
0	monoclinic	a_m = 5.150 b_m = 5.207 c_m = 5.318 β = 99.22	27
	tetragonal	a = 5.086[a] c = 5.177	20
10	tetragonal	a = 5.122[a] c = 5.218	12.8
20	tetragonal	a = 5.158[a] c = 5.254	9.2
30	tetragonal	a = 5.197[a] c = 5.265	10
40	tetragonal	a = 5.230[a] c = 5.288	9.6
50	tetragonal[b]	A = 5.3016	9.6
60	tetragonal[b]	a =5.325	8.3
70	tetragonal[b]	a =5.345	8.4
80	tetragonal[b]	a = 5.360	8.5
90	cubic	a = 5.389	16
100	cubic	a =5.411	23

[a]The lattice parameters of pseudofluorite cell.

[b]Axial ratio c/a =1; from XRD pattern this phase is commonly indexed in the *Fm*3*m* space group.

[c]Crystallite size calculated from XRD.

Nanophase powders are a new class of materials which, in contrast to conventional solids, have an appreciable fraction of their atoms residing in defected environments,

especially on grain boundaries, where they occupy positions relaxed from their normal lattice sites [52]. Therefore the properties of nanophase materials are strongly related to their unique microstructures. This additional line broadening due to sample effects results from two main effects: the particle-size which results from the finite extent and particular morphology of the coherently diffracting domains within the grains, and the microstrain broadening or possibly defected structure. The precise determination of microstructural parameters requires taking into account strain and size effects in order to achieve the best interpretation of the observed peak-profile broadening.

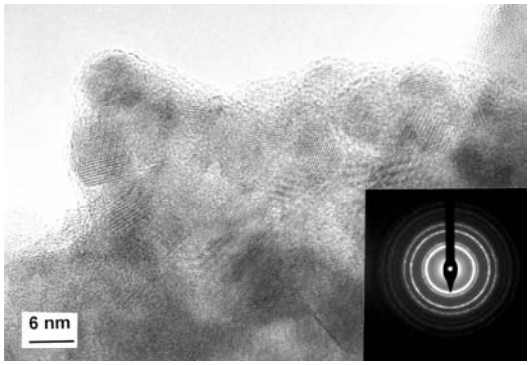

Fig. 4. HRTEM micrograph of the $Ce_{0.4}Zr_{0.6}O_2$ sample heated in air at 600 °C for 16 h and corresponding electron diffraction pattern (inset)

In order to observe a real microstructure of $Ce_xZr_{(1-x)}O_2$ samples heat-treated in air at 600 °C for 16 h we used TEM studies. HRTEM observations obtained for the 40 mol % CeO_2 sample (a representative image is given in Fig. 4) show the presence of nanocrystalline particles with lattice fringes corresponding to the (111) lattice plane in fluorite structure. These particles appear with narrowly distributed sizes, around 8–9 nm, thus corresponding roughly to the crystallite sizes detected in XRD. Specific preferential crystal orientations were not observed. The dried sample was composed of highly aggregated ultrafine particles.

A selected area electron diffraction pattern was also taken from this material (inset in Fig. 4). It shows the Debye–Sherrer rings (somewhat grainy, indicating incomplete sampling of all possible orientations) that can be consistently indexed according to a cubic fluorite structure with the lattice parameter of 5.25 Å. This value is in a relatively good agreement with XRD results. However, the positions of the rings agreed with those expected for the fluorite structure, although their line widths are too large to allow the presence of some tetragonal character to be excluded.

Vibrational spectroscopy is an effective tool for identification of the phase composition in the binary Ce–Zr–O system [10, 47, 48, 53–57]. Raman scattering measurements are more powerful than the XRD method for detection of a small amount of the stable tetragonal phase mixed with the cubic phase. Therefore Raman spectra can be used to characterize the CeO_2–ZrO_2 solid solution samples.

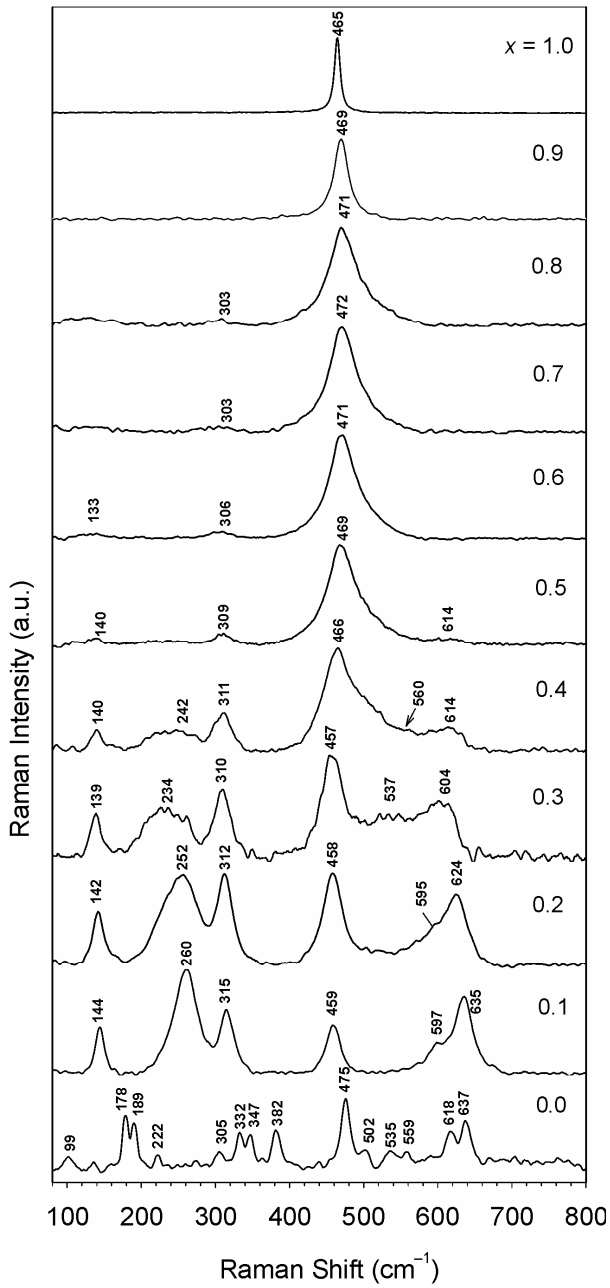

Fig. 5. Raman spectra of $Ce_xZr_{(1-x)}O_2$ samples after heat-treatment in air at 600 °C for 16 h

From the theoretical point of view the following vibrational characteristics are predicted for the respective phases of zirconia [58, 59]. For the cubic phase of the

fluorite structure (space group $Fm3m \equiv O_h^5$, $Z = 1$) the irreducible representation of the optic phonons is F_{2g} (R) + F_{1u} (IR).

For tetragonal t-ZrO_2 (space group $P4_2/nmc \equiv D_{4h}^{15}$, $Z = 2$) the distribution of the normal modes is: A_{1g} (R) + $2B_{1g}$ (R) + $3E_g$ (R) + A_{2u} (IR) + $2E_u$ (IR). In monoclinic phase (space group $P2_1/c \equiv C_{2h}^5$, $Z = 4$) all atoms lie on general positions and therefore the expected IR and Raman active modes are as follows: $9A_g$ (R) + $9B_g$ (R) + $8A_u$ (IR) + $7B_u$ (IR).

In XRD patterns, the peak broadening due to a small size of the crystallites makes detection of the tetragonal phase difficult, whereas the t phase exhibits six relatively strong, narrow bands in the Raman spectra as compared with one strong band for the cubic phase. However, for t″- or t′-phase only four or five modes could be visible at intermediate ceria contents (40–60 % mol). Besides strong bands at 465 cm^{-1} with a weak broad shoulder at about 550 cm^{-1} some very weak peaks at about 145 and 310 cm^{-1} are also observed [10, 42]. This high-frequency tail at 550 cm^{-1} has been attributed to oxygen vacancies [57]. Keeping in mind these theoretical predictions, the Raman spectra of the samples have been discussed.

Figure 5 shows the Raman spectra of $Ce_xZr_{(1-x)}O_2$ solid solution after calcination in air at 600 °C for 16 h. As expected, in pure CeO_2 only a strong F_{2g} mode is observed at 465 cm^{-1}. For $Ce_xZr_{(1-x)}O_2$ (x = 0.5–0.9) samples, the spectrum is dominated by a single strong band which shifts to higher frequencies (470 cm^{-1}). It has a very broad and asymmetric profile. Additionally, some peaks of low intensities at about 139 and 310 cm^{-1} are visible, indicating that t″-phase is also present. For $Ce_xZr_{(1-x)}O_2$ ($x < 0.4$) samples six bands of the tetragonal t-phase have been detected. For pure ZrO_2 the Raman spectrum shows a typical monoclinic phase without evidence of minor t-ZrO_2 phase.

Zhang et al. [60] reported recently that additional effects in Raman spectra should be expected for pure CeO_2 nanoparticles when the particle size is smaller than 20 nm. The peak at 464 cm^{-1} shifts to lower energies and shows large asymmetric broadening with decreasing particle size. The lattice expansion with decreasing particle size largely explains this systematic change of the Raman peak which can be attributed to the increasing concentration of point defects. The crystallite size effect (6–15 nm) on Raman spectra of undoped nanocrystalline tetragonal zirconia was presented by Djurado et al. [40]. Vibrational properties of nanomaterials are strongly dependent on the nano-grain size. In general, one can expect a broadening and frequency shifting of Raman bands as the nanograin size decreases.

3.4. Structural changes due to heat-treatment at 1100 °C in air and in reducing conditions

XRD patterns of $Ce_xZr_{(1-x)}O_2$ samples heated in air up to 1100 °C for 16 h are shown in Fig. 6. The $Ce_xZr_{1-x}O_2$ (x = 0.2–0.8) samples heated above 1000 °C show

considerable phase separation. According to the phase diagram in this system, there exists a wide two-phase (t + c) region. During annealing in air at 1100 °C for 16 h, the $Ce_xZr_{1-x}O_2$ (x = 0.2–0.8) solid solution separated into tetragonal phase with lower CeO_2 concentration (t-$Ce_{0.16}Zr_{0.84}O_2$; a = 5.1445 Å, c = 5.2394 Å) and the cubic phase with higher CeO_2 concentration (c-$Ce_{0.75}Zr_{0.25}O_2$; a = 5.347Å).

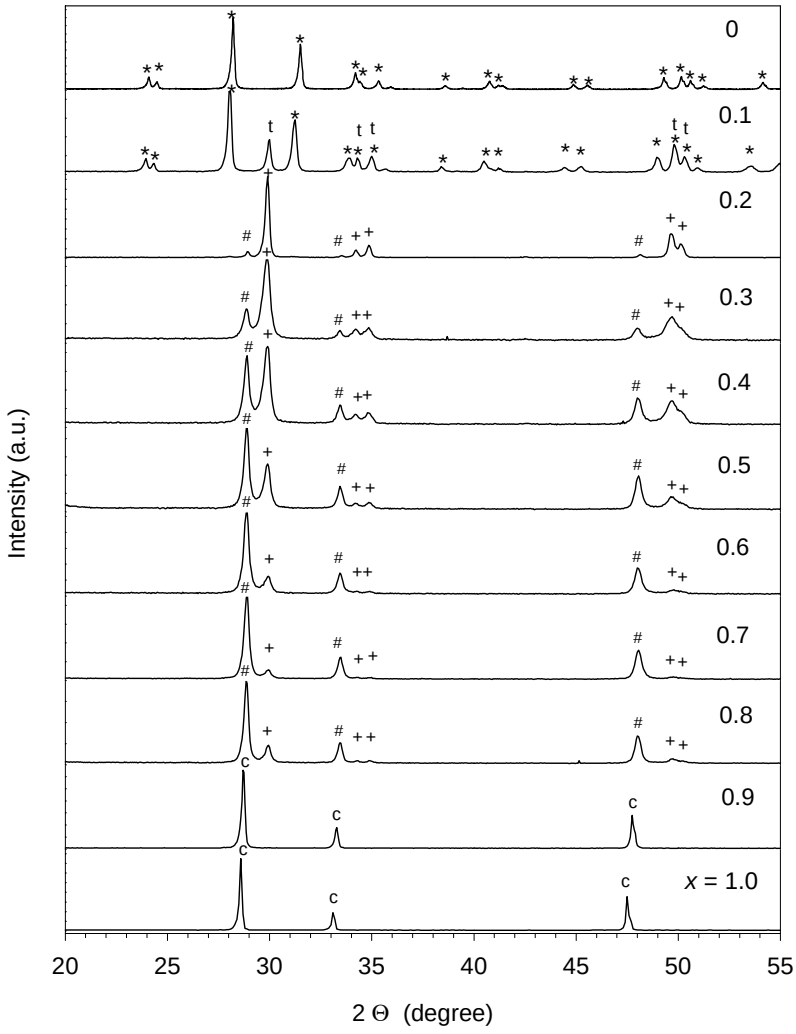

Fig. 6. X-ray diffraction patterns of $Ce_xZr_{(1-x)}O_2$ samples heated in air at 1100 °C for 16 h. The symbols (*) (t) (c) (#) and (+) indicate most intense lines of the monoclinic, tetragonal, cubic $Ce_xZr_{(1-x)}O_2$ phases and c-($Ce_{0.75}$ $Zr_{0.25}O_2$) , t-($Ce_{0.16}Zr_{0.84}O_2$) phases, respectively

The Raman spectra for $Ce_{0.3}Zr_{0.7}O_2$ and $Ce_{0.5}Zr_{0.5}O_2$ solid solution samples calcined at different temperatures (600 and 1100 °C) and in different atmospheres (air and 5% H_2/He) are presented in Figs. 7 and 8, respectively. The Raman spectra of

initial tetragonal t-$Ce_{0.3}Zr_{0.7}O_2$ and t″-$Ce_{0.5}Zr_{0.5}O_2$ homogeneous solid solution samples calcined at 600 °C for 16 h are presented in Fig. 7a and 8a, respectively. After calcination at 1100 °C in air both initial samples are composed of two phases (t-$Ce_{0.16}Zr_{0.84}O_2$ and c-$Ce_{0.75}Zr_{0.25}O_2$) with different relative concentrations. Their Raman spectra (Figs. 7b and 8b) consist of multiplets characteristic of the t- and c-phases. The existence of c-$Ce_{0.75}Zr_{0.25}O_2$

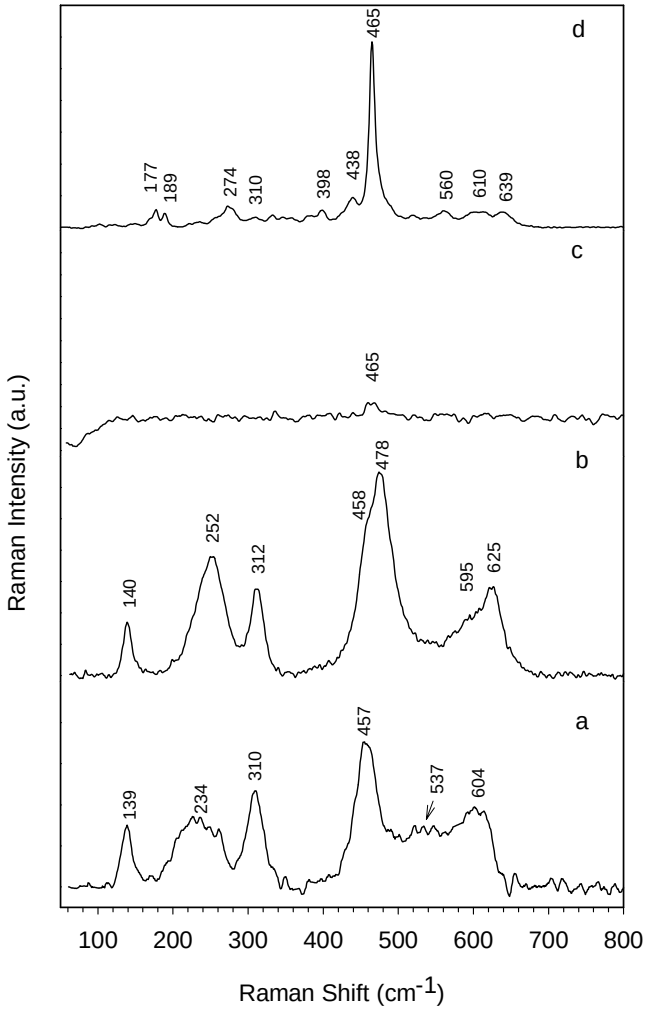

Fig. 7. Raman spectra of $Ce_{0.3}Zr_{0.7}O_2$ samples: a) heated in air at 600 °C for 16 h; b) heated in air at 1100 °C for 16 h; c) heated in 5% H_2/He gas mixture at 1100 °C for 10 h, d) heated in 5% H_2/He gas mixture at 1100 °C and subsequent calcination in air at 600 °C

phase is confirmed by the very strong line at 478 cm^{-1} and for t-$Ce_{0.16}Zr_{0.84}O_2$ phase Raman lines appears at about 625, 595, 458, 312, 252, 140 cm^{-1}. In pure CeO_2, the F_{2g} mode is observed at 465 cm^{-1} and for c-ZrO_2 the F_{2g} mode is centred at 490 cm^{-1} [47].

With decreasing CeO_2 content (down to about 60% mol) this single F_{2g} mode for cubic phase becomes broader and shifts to higher frequencies due to a decrease of the cubic lattice parameter [10]. The only difference between these Raman spectra (Figs. 7b and 8b) is a much higher intensity of the F_{2g} mode at 478 cm^{-1} for sample with the initial composition of $Ce_{0.5}Zr_{0.5}O_2$ (Fig. 8b), which is related to a higher content of the cubic (c-$Ce_{0.75}Zr_{0.25}O_2$) phase in the sample.

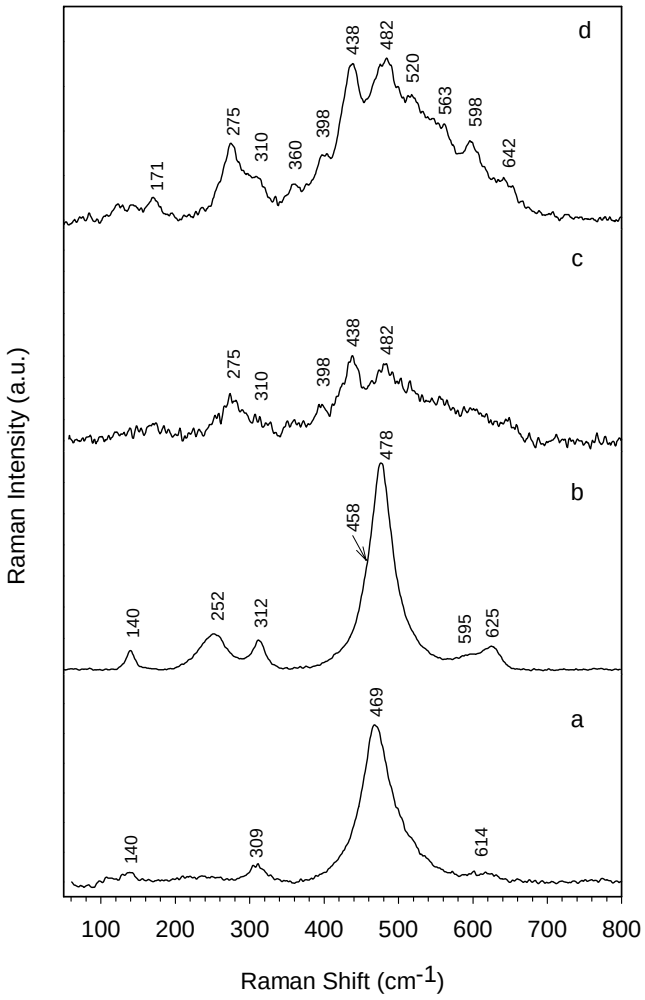

Fig. 8. Raman spectra of $Ce_{0.5}Zr_{0.5}O_2$ samples: a) heated in air at 600 °C for 16 h; b) heated in air at 1100 °C for 16 h; c) heated in 5% H_2/He gas mixture at 1100 °C for 10 h and d) heated in 5% H_2/He gas mixture at 1100 °C and subsequently calcinated in air at 600 °C

Raman scattering measurements also provided a supplementary evidence for the phase separation in samples reduced with hydrogen at 1100 °C. Figures 7c and 8c show Raman spectra for H_2 reduced initial $Ce_{0.3}Zr_{0.7}O_2$ and $Ce_{0.5}Zr_{0.5}O_2$ samples, re-

spectively. The Raman spectrum of reduced $Ce_{0.3}Zr_{0.7}O_2$ sample consists of only one very weak line observed at 465 cm^{-1}. Also, the spectrum of the reduced $Ce_{0.5}Zr_{0.5}O_2$ sample (Fig. 8c) is significantly more complex, consisting of very broad and weak lines of the disordered new phase (275, 310, 398, 438, 482 cm^{-1}). It is well known [61] that Raman spectra of disordered phases show less-resolved, broad lines resulting from the order defects (anion vacancies, antiphase boundaries, substituted cations). However, it could be possible to recognize defective cubic κ-Ce–Zr–O solid solutions which are formed after oxidation of the $Ce_2Zr_2O_{7+\delta}$ pyrochlore phase at ambient temperature. The Raman spectrum of non-defective cubic κ-phase, obtained by subsequent reoxidation at 600 °C in air of H_2 reduced $Ce_{0.5}Zr_{0.5}O_2$ sample at 1100 °C, is shown in Fig. 8d. These Raman bands are in a good accordance with the literature data [62, 63]. The Raman spectrum of non-defective $Ce_{0.3}Zr_{0.7}O_2$ sample prepared by hydrogen reduction and subsequent reoxidation at 600 °C is shown in Fig. 7d. After reoxidation the following phases are identified: cubic (465 cm^{-1}); κ-phase (274, 398, 438, 560, 610, 639 cm^{-1}) and monoclinic phase (177, 189 cm^{-1}).

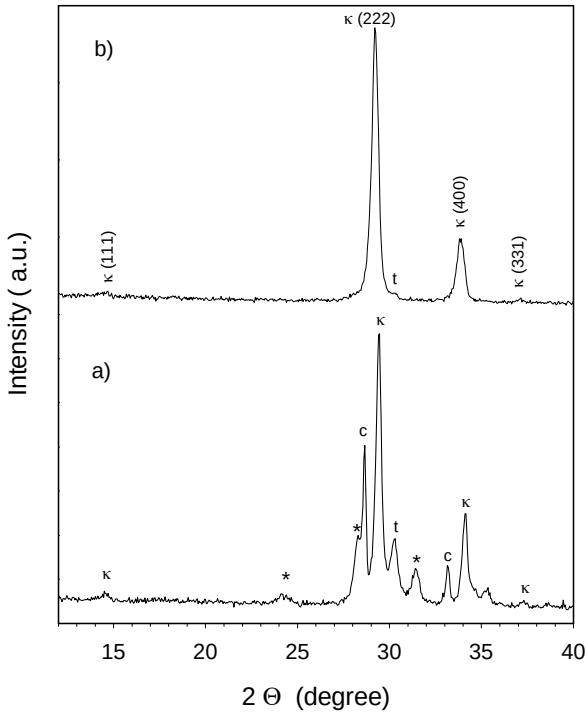

Fig. 9. X-ray diffraction patterns of $Ce_xZr_{(1-x)}O_2$ samples reduced in 5% H_2/He gas mixture at 1100 °C for 10 h: a) x = 0.3, b) x = 0.5. The symbols (*) (c) (t) and (κ) indicate most intense lines of the monoclinic, cubic, tetragonal and cubic κ-phase, respectively

The phase compositions of hydrogen reduced samples at 1100 °C were also investigated by XRD. The corresponding diffraction patterns are compared in Fig. 9. The

$Ce_xZr_{1-x}O_2$ ($x \approx 0.1$–0.3) samples consist of four phases. The exemplary XRD pattern for the reduced $Ce_{0.3}Zr_{0.7}O_2$ sample (Fig. 9a) exhibits very complex behaviour with extensive peak overlapping. After profile fitting of the XRD pattern, the major $Ce_xZr_{(1-x)}O_{2-\delta}$ phase could be indexed in the cubic pyrochlore cell with lattice parameter a = 10.520 Å. A low-intensity (odd, odd, odd) reflections confirm the cubic pyrochlore-type phase. The minor phases are low Ce-doped zirconia: t-ZrO_2 (a = 5.091 Å, c = 5.18 Å), m-ZrO_2 (a = 5.155 Å, b = 5.197 Å, c = 5.320 Å, β = 98.87°) and almost pure c-CeO_2 (a = 5.40 Å). However, these phases must have a very disordered oxygen sublattice as is evidenced from their Raman spectra (Fig. 7c).

The XRD patterns for the reduced $Ce_{0.5}Zr_{0.5}O_2$ sample after heat-treatment in hydrogen at 1100 °C are shown in Fig. 9b. It is interesting to note that no phase separation occurs during reductive heat treatment for this composition. The XRD pattern for this solid solution was indexed on the basis of a cubic pyrochlore-related structure with the lattice constant a = 10.584 Å. Only traces of tetragonal phase (2Θ =30.2°) could be noticed.

The phase separation in the Ce–Zr–O system induced by heat treatment in a reducing gas should be interpreted with regard to the ternary ZrO_2–CeO_2–$CeO_{1.5}$ phase diagram [64, 65].

The formation of a cubic κ-phase after a cycling of high-temperature reduction and subsequent oxidation is very effective to the enhancement of the oxygen storage capacity (OSC) and to decrease the reduction temperature in comparison with starting t′-tetragonal solid solution [63].

4. Conclusion

The polymerized complex method produces excellent precursors yielding nanocrystalline homogeneous ceria–zirconia solid solutions at low temperatures and for shorter annealing times, reducing segregation of the components. XRD, HRTEM, TG-DTA and Raman measurements have been successfully carried out on the polymeric derived CeO_2–ZrO_2 mixed oxides samples. The success in lowering the crystallization temperature of mixed oxides to about 250 °C may indicate an improved level of mixing of the cations in the prepared samples. The phase composition and the reduction properties of $Ce_xZr_{(1-x)}O_2$ solid solution depend on the choice of preparation method and specific processing conditions. To our best knowledge, no lower decomposition temperature was reached by the polymerized complex methods.

However, during a prolonged heat treatment in air or in a reducing gas at 1100 °C, phase segregation to more thermodynamically stable phases was observed. The $Ce_{0.5}Zr_{0.5}O_2$ solid solution shows lower thermal stability in air and slight phase segregation in hydrogen at 1100 °C in comparison to $Ce_{0.3}Zr_{0.7}O_2$ sample. Raman spectroscopy provided sufficient evidence for the phase separation even at the initial stage where XRD was not successful in showing the tetragonal components in the cubic

matrix. It is very important to investigate the thermal stability of the solid solutions prepared by the polymer route, particularly for use as advanced materials for the three-way catalyst (TWC-s) applications.

Acknowledgements

Financial support for this research programme from The Royal Society Postdoctoral Fellowship is greatly appreciated. The authors thank Dr. L. Kępiński and L. Krajczyk for performing HRTEM image and Z. Mazurkiewicz for skilful technical assistance.

References

[1] TROVARELLI A., Catal. Rev.-Science & Engineering, 38 (1996), 439.
[2] OZAWA M., J. Alloys Comp., 257–277 (1998), 886.
[3] FORNASIERO P., BALDUCCI G., KAŠPAR J., MERIANI S., DI MONTE R., GRAZIANI M., Catal. Today, 29 (1996), 47.
[4] DI MONTE R., KASPAR J., Topics Catal., 28 (2004), 47.
[5] SUGIURA M., Catal. Surveys Asia, 7 (2003), 77.
[6] BERNAL S., BLANCO G., CALVINO J.J., GATICA J.M., PEREZ-OMIL J.A., PINTADO J.M., Topics Catal., 28 (2004), 31.
[7] KASPAR J., FORNASIERO P., J. Solid State Chem., 171 (2003), 19.
[8] VLAIC G., DI MONTE R., FORNASIERO P., FONDA E., KASPAR J., GRAZIANI M., Studies Surface Sci. Catalysis, 116 (1998), 185.
[9] YASHIMA M., SASAKI S., YAMAGUCHI Y., KAKIHANA M., YOSHIMURA M., MORI T., Appl. Phys. Lett., **7**2 (1998), 182.
[10] VLAIC G., DI MONTE R., FORNASIERO P., FONDA E., KASPAR J., GRAZIANI M., J. Catal., 182 (1999), 378.
[11] LEITENBURG C., TROVARELLI A., ZAMAR F., MASCHIO S., DOLCETTI G., LLORCA J., J. Chem. Soc. Chem. Commun. (1995), 2181.
[12] SUDA A., KANDORI T., TERAO N., UKYO Y., SOBUKAWA H., SUGIURA M., J. Mater. Sci. Lett., 17 (1998), 89.
[13] LIN J.-D., DUH J.-G., J. Am. Ceram. Soc., 80 (1997), 92.
[14] HIRANO S., KAWABATA A., YOSHINAKA M., HIROTA K., YAMAGUCHI O., J. Am. Ceram. Soc., 78 (1995), 1414.
[15] SUN Y., SERMON P.A., J. Mater. Chem., 6 (1996), 1025.
[16] KAWABATA A., HIRANO S., YOSHINAKA M., HIROTA K., YAMAGUCHI O., J. Mater. Sci., 31 (1996), 4945.
[17] ROSSIGNOL S., MADIER Y., DUPREZ D., Catal. Today, 50 (1999), 261.
[18] HIRANO M., KATO E., J. Am. Ceram. Soc., 104 (1996), 958.
[19] CABANAS A., DARR J.A., LESTER E., POLIAKOFF M., Chem. Comm. (2000), 901.
[20] CABANAS A., DARR J.A., LESTER E., POLIAKOFF M., J. Mater. Chem., 11 (2001), 561.
[21] KAPOOR M.P., RAJ A., MATSUMURA Y., Micropor. Mesopor. Mater., 44–45 (2001), 565.
[22] YOSHIOKA T., DOSAKA K., SATO T., OKUWAKI A., TANNO S., MIURA T., J. Mater. Sci. Lett., 11 (1992), 51.
[23] KAKIHANA M., KATO S., YASHIMA M., YOSHIMURA M., J. Alloys Comp., 280 (1998), 125.
[24] SETTU T., GOBINATHAN R., Bull. Chem. Soc. Jpn., 67 (1994), 1999.
[25] ARUNA S.T., PATIL K.C., Nanostr. Mater., 10 (1998), 955.
[26] PRAKASH A.S., KHADAR A.M.A., PATIL K.C., HEGDE M.S., J. Mater. Synth. Process., 10 (2002), 135.
[27] LUO M.-F., LU G.-L., ZHENG X.-M., J. Mater. Sci. Lett., 17 (1998), 1553.
[28] MASUI T., FUJIWARA K., PENG Y., SAKATA T., MACHIDA K., MORI H., ADACHI G., J. Alloys Comp., 269 (1998), 116.
[29] MARTINEZ-ARIAS A., FERNANDEZ-GARCIA M., BALLESEROS V., SALAMANCA L.N., CONESA J.C., OTERO C., SORIA J., Langmuir, 15 (1999), 4796.

[30] PECHINI M.P., US Pat. 3, 330, 697 (1967).
[31] YASHIMA M., OHTAKE K., KAKIHANA M., YOSHIMURA M., J. Am. Ceram. Soc., 77 (1994), 2773.
[32] QUINELATO A.L., LONGO E., LEITE E.R., VARELA J.A., Appl. Organom. Chem., 13 (1999), 501.
[33] YAMAMOTO S., KAKIHANA M., KATO S., J. Alloys Comp., 297 (2000), 81.
[34] CHEN C.C., NASRALLAH M.M., ANDERSON H.U., J. Electrochem. Soc., 140 (1993), 3555.
[35] CHEN C.C., NASRALLAH M.M., ANDERSON H.U., Solid State Ionics, 70-71 (1994), 101.
[36] YOUNG R.A., SAKTHIVEL A., MOSS T.S., PAIVA-SANTOS C.O., J. Appl. Cryst., 28 (1995), 366.
[37] KRAUS W., NOLZE G., *PowderCell* software, Federal Institute for Materials Research and Testing, 12489 Berlin, Germany.
[38] MIMANI T., PATIL K.C., Mater. Phys. Mech., 4 (2001), 134.
[39] NARENDAR Y., MESSING G.L., Catal. Today, 35 (1997), 247.
[40] DJURADO E., BOUVIER P., LUCAZEAU G., J.Solid State Chem., 149 (2000), 399.
[41] KASPAR J., FORNASIERO P., GRAZIANI M., Catal. Today, 50 (1999), 285.
[42] FORNASIERO P., BALDUCCI G., DI MONTE R., KASPAR J., SERGO V., GUBITOSA G., FERRERO A., GRAZIANI M., J. Catal., 164 (1996), 173.
[43] YASHIMA M., ARASHI H., KAKIHANA M., YOSHIMURA M., J. Am. Ceram. Soc., 77 (1994), 1067.
[44] YASHIMA M., MORIMOTO K., ISHIZAWA N., YOSHIMURA M., J. Am. Ceram. Soc., 76 (1993), 2865.
[45] YASHIMA M., MORIMOTO K., ISHIZAWA N., YOSHIMURA M., J. Am. Ceram. Soc., 76 (1993), 1745.
[46] MERIANI S., SPINOLO G., Powder Diffract., 2 (1987), 255.
[47] KASPAR J., FORNASIERO P., BALDUCCI G., DI MONTE R., HICKEY N., SERGO V., Inorg. Chim. Acta, 349 (2003), 217.
[48] ESCRIBANO V.S., LOPEZ E.F., PANIZZA M., RESINI C., AMORES J.M.G., BUSCA G., Solid State Science, 5 (2003), 1369.
[49] TROVARELLI A., BOARO M., ROCCHINI E., LEITENBURG C., DOLCETTI G., J. Alloys Comp., 323–324 (2001), 584.
[50] YASHIMA M., YOSHIMURA M., Mater. Jpn, 34 (1995), 448.
[51] YASHIMA M., YOSHIMURA M., Jpn. J. Appl. Phys., 31 (1992), L1614.
[52] *Nanomaterials: synthesis, properties and applications*, A.S. Edelstein, R.C. Cammarata (Eds.), Institute of Physics Publishing, Bristol, 1995, p. 201.
[53] COLON G., PIJOLAT M., VALIVIESO F., VIDAL H., KASPAR J., FINOCCHIO E., DATURI M., BINET C., LAVALLEY J.C., BAKER R.T, BERNAL S., J. Chem. Soc. Faraday Trans., 94 (1998), 3717.
[54] DI MONTE R., FORNASIERO P., GRAZIANI M., KASPAR J., J. Alloys Compd., 275–277 (1998), 877.
[55] HIRATA T., ZHU H., FURUBAYASHI T., NAKATANI I., J. Am. Ceram. Soc., 76 (1993), 1361.
[56] HIRATA T., ZHU H., Solid State Commun., 80 (1991), 991.
[57] FORNASIERO P., KASPAR J., SERGO V., GRAZIANI M., J. Catal., 182 (1999), 56.
[58] HIRATA T., ASARI E., KITAJIMA M., J. Solid State Chem., 110 (1994), 201.
[59] YASHIMA M., OHTAKE K., KAKIHANA M., ARASHI H., YOSHIMURA M., J. Phys. Chem. Solids, 57 (1996), 17.
[60] ZHANG F., CHAN S.-W., SPANIER J.E., APAK E., JIN Q., ROBINSON R.D., HERMAN I.P., Appl. Phys. Letters, 80 (2002), 127.
[61] MICHEL D., JORBA M.P.Y, COLLONGUES R., J. Raman Spectr., 5 (1976), 163.
[62] OTSUKA-YAO-MATSUO S., OMATA T., IZU N., KISHIMOTO H., J. Solid State Chem., 138 (1998), 47.
[63] MASUI T., OZAKI T., MACHIDA K., ADACHI G., J. Alloys Comp., 303–304 (2000), 49.
[64] IZU N., OMATA T., OTSUKA-YAO- S., J. Alloys Comp., 270 (1998), 107.
[65] OTSUKA-YAO-MATSUO S., MORIKAWA H., IZU N., OKUDA K., J. Japan Inst. Metals, 59 (1995), 1237.

Received 16 April 2004
Revised 22 June, 2004